Cell Reports, Volume *23*

Supplemental Information

Active Zone Scaffold Protein Ratios Tune Functional Diversity across Brain Synapses

Andreas Fulterer, Till F.M. Andlauer, Anatoli Ender, Marta Maglione, Katherine Eyring, Jennifer Woitkuhn, Martin Lehmann, Tanja Matkovic-Rachid, Joerg R.P. Geiger, Alexander M. Walter, Katherine I. Nagel, and Stephan J. Sigrist

Supplemental Information

Supplemental Data Items

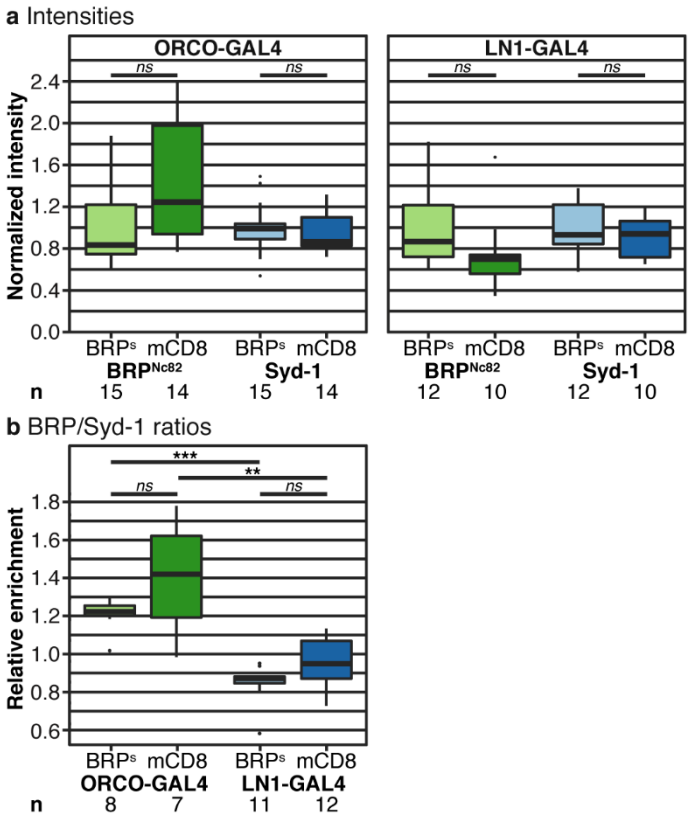

Figure S1: Expression of *brp-short* does not significantly alter the intensities or ratios of scaffold proteins, related to Figure 1

Analysis of staining intensities and antibody ratios. Either brp-short-GFP or mCD8-GFP was expressed using either ORCO-GAL4 (left) or LN1-GAL4 (right). Sample sizes (n) are indicated at the bottom of the plots.

(a) Average staining intensities of BRP and Syd-1 in ALs. For each driver line, normalized intensities of BRP and Syd-1 did not significantly differ between the two GFP fusion proteins used. Average intensities for mCD8-GFP were normalized to BRP-short-GFP intensities. Association tests were conducted using linear mixed models with imaging batch and animal as nested random effects. The Bonferroni-corrected significance threshold was $\alpha = 0.025$ for each GAL4 line. ORCO-GAL4: BRP^{Nc82} $p = 0.15$, Syd-1 $p = 0.58$; LN1-GAL4: BRP^{Nc82} $p = 0.13$, Syd-1 $p = 0.39$. BRPs = BRP-short.

(b) Analysis of median BRP/Syd-1 ratios in ALs. GFP-positive median ratios were normalized by median ratios of the surrounding AL to illustrate the relative difference between GFP-positive AZs and the surrounding AL. The AZs positive for ORCO-GFP were enriched for BRP in comparison to LN1-derived AZs using either GFP fusion protein; significance tests were carried out using Mann-Whitney U tests. BRP-short-GFP: $p = 0.0000265$, mCD8-GFP: $p = 0.00179$. No significant difference was observed between BRP-short-GFP- and mCD8-GFP-based ratios: ORCO-GAL4: $p = 0.189$, LN1-GAL4: $p = 0.0595$. The Bonferroni-corrected significance threshold was $\alpha = 0.05/4 = 0.0125$.

Graphs show medians, interquartile ranges, and min/max values.

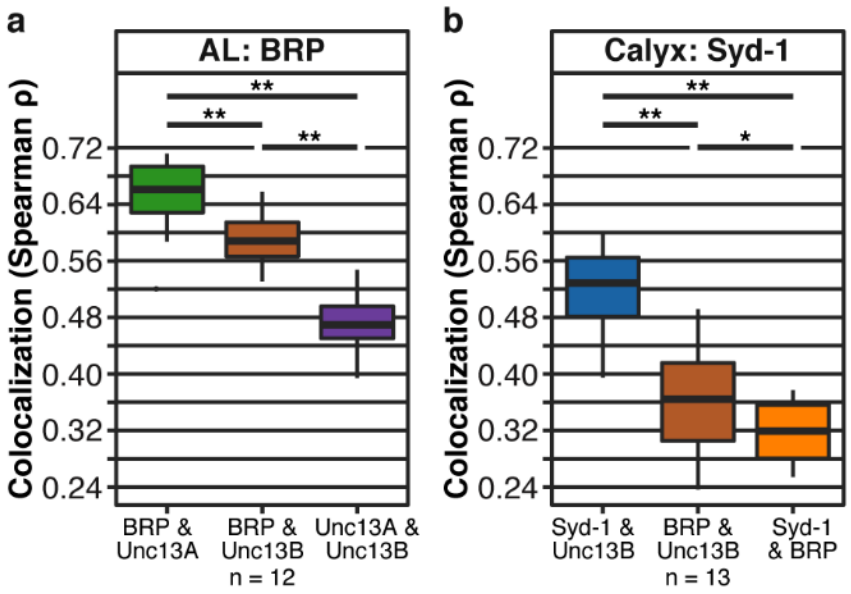

Figure S2: Colocalization analysis of the scaffold proteins BRP/Syd-1 and the Unc13 isoforms Unc13A/Unc13B, related to Figure 1 and Figure 2

Colocalization analysis using the Fiji Coloc 2 plugin (Spearman correlation) was conducted to examine pixel intensity correlations over space in single confocal images. We analyzed two separate sets of triple stainings, based on the available antibody combinations. All significance tests were carried out using the paired Wilcoxon signed-rank test. The Bonferroni-corrected significance threshold was $\alpha = 0.05/3 = 0.0167$ for each staining group. Sample sizes (n) are indicated at the bottom of the plots.

(a) BRP^{Nc82}, Unc13A, Unc13B triple staining analyzed in the AL where BRP^{Nc82} showed a heterogeneous distribution. The colocalization of BRP^{Nc82} and Unc13A was significantly higher than the colocalization of either BRP^{Nc82} and Unc13B ($p = 0.00049$) or Unc13A and Unc13B ($p = 0.00049$); the colocalization of BRP^{Nc82} and Unc13B was significantly higher than the one of Unc13A and Unc13B ($p = 0.00049$).

(b) Syd-1, BRP^{Nc82}, Unc13B triple staining analyzed in the calyx where Syd-1 showed a heterogeneous distribution. The colocalization of Syd-1 and Unc13B was significantly higher than the colocalization of either BRP^{Nc82} and Unc13B ($p = 0.00024$) or Syd-1 and BRP^{Nc82} ($p = 0.00024$); the colocalization of BRP^{Nc82} and Unc13B was significantly higher than the one of Syd-1 and BRP^{Nc82} ($p = 0.0017$).

Graphs show medians, interquartile ranges, and min/max values.

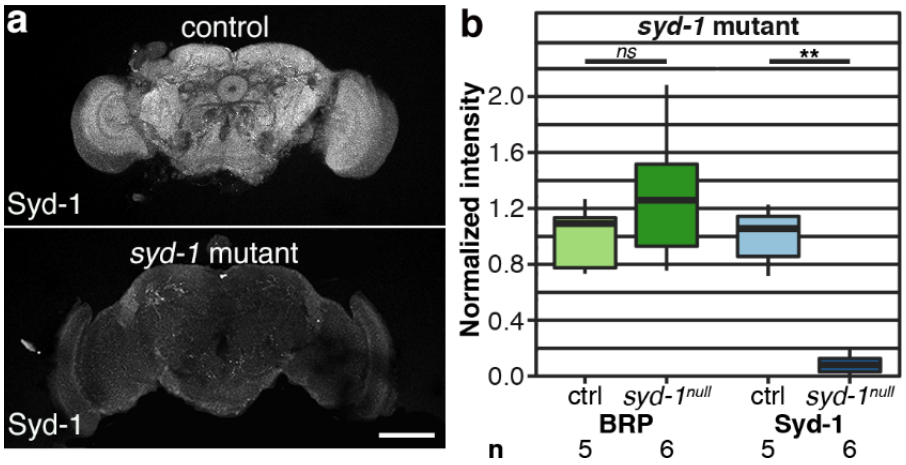

Figure S3: Quantification of the antibody staining reduction in *syd-1* null mutants in the adult *Drosophila* brain, related to Figure 3

(a) Confocal images of *Drosophila* central brains of *syd-1* mutant flies (*syd-1*$^{ex1.2}$/*syd-1*$^{ex3.4}$) in comparison to *w*^{1118} controls, stained against Syd-1; scale bar: 100 μm.

(b) Analysis of average staining intensities of BRP^{Nc82} and Syd-1 in *syd-1* mutants normalized to controls (ctrl). Average intensity levels of Syd-1 were significantly downregulated to 8.7 % of control levels ($p = 0.0013$). BRP^{Nc82} levels were not altered ($p = 0.25$). Association tests were conducted using a permutation test (10,000 permutations), based on linear mixed models with the imaging batch as a random effect. The permutation test was carried out because the residuals of the regression were not normally distributed. The Bonferroni-corrected significance threshold was $\alpha = 0.025$. Sample sizes (n) are indicated at the bottom of the plots. The graph shows medians, interquartile ranges, and min/max values.

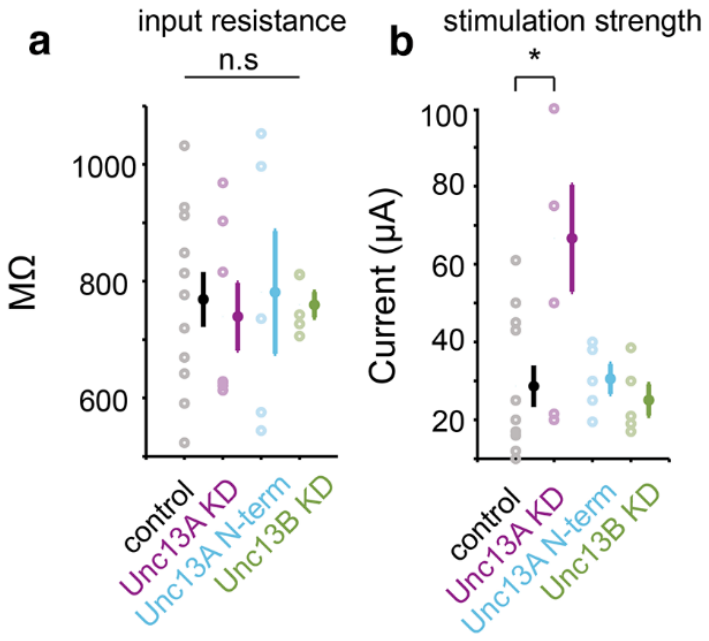

Figure S4: PN input resistances are similar across control and *unc13A/B* KD flies, related to Fig. 5
(a) Input resistance.
(b) Stimulation current at the antennal nerve necessary to evoke EPSCs at the downstream PNs. *unc13A* KD: pb-GAL4>UAS-*unc13A*-RNAi-A1; *unc13B* KD: pb-GAL4>UAS-*unc13B*-RNAi-B3; *unc13A* N-term: pb-GAL4>UAS-*unc13A-N-term-GFP*. An increased current was required to elicit responses in the *unc13A* KD flies compared to controls ($p < 0.01$; unpaired Student's t-test). Mean values ± SEM are represented.

.

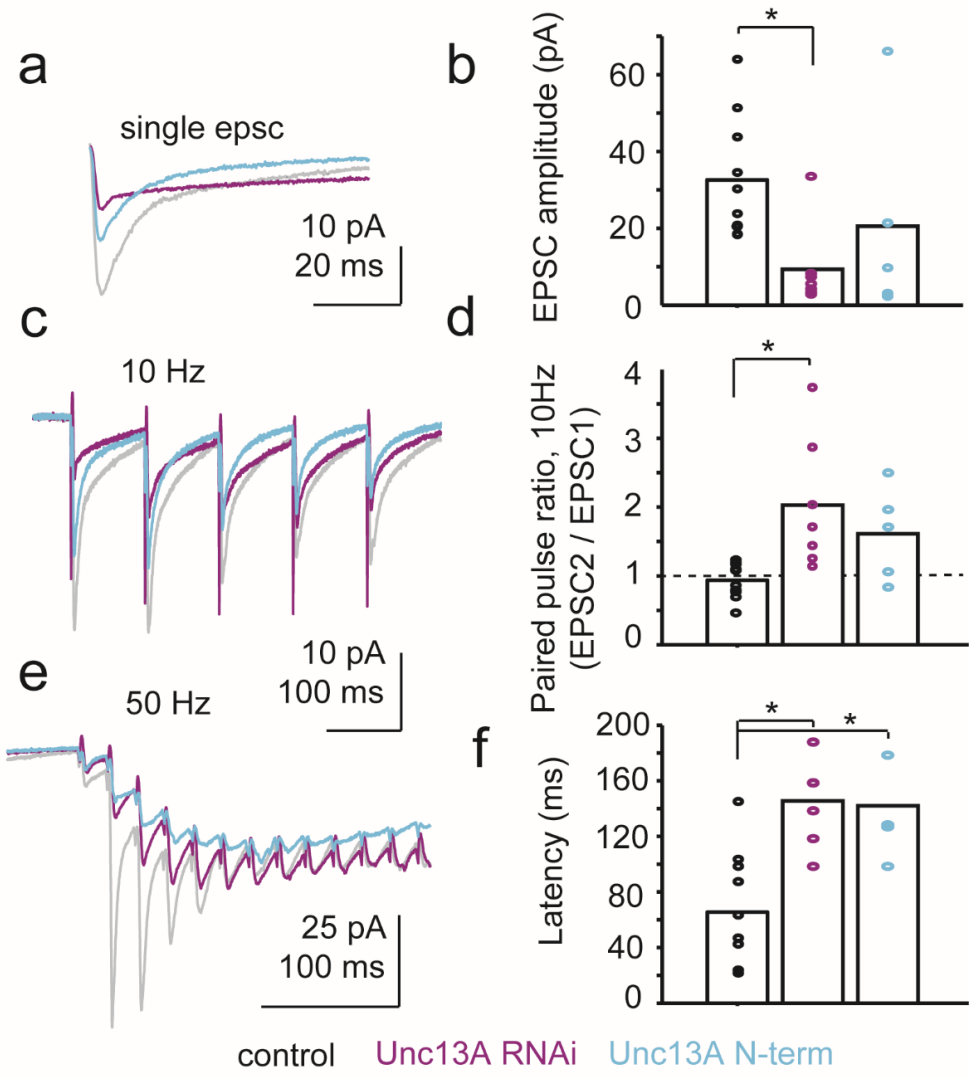

Figure S5: Loss of Unc13A by either RNAi-mediated knockdown or overexpression of a dominant-negative construct produces similar effects at the ORN-PN synapse, related to Figure 5
(a) Group-averaged single EPSCs; control (n = 10 cells), *unc13A* KD (n = 7 cells), *unc13A* dominant negative (DN, n = 5 cells). **(b)** Quantification of EPSC amplitudes across genotypes. EPSC amplitudes differed between genotypes ($F = 3.71$, $p < 0.05$, one-way ANOVA with Tukey post-hoc comparison). EPSCs were significantly smaller in *unc13A* KD flies compared to controls ($p < 0.01$, unpaired Student's t-test). **(c)** Group-averaged EPSCs evoked by 10 Hz stimulation; control (n = 10 cells), *unc13A* KD (n = 7 cells), *unc13A* DN (n = 5 cells). **(d)** Quantification of the paired-pulse ratio (PPR) between first and second EPSCs across genotypes. PPRs were different between genotypes ($F = 6.16$, $p < 0.01$, one-way ANOVA with Tukey post-hoc comparison). EPSCs were significantly smaller in *unc13A* KD flies compared to controls ($p < 0.01$, unpaired Student's t-test). **(e)** Group-averaged EPSCs evoked by 50 Hz stimulation; control (n = 10 cells), *unc13A* KD (n = 7 cells), *unc13A* DN (n = 5 cells). **(f)** Quantification of latency to peak current evoked by 50 Hz stimulation across genotypes. The latency, which was quantified as the time between the onset of 50 Hz stimulation and the peak evoked current, differed between genotypes ($F = 12.29$, $p < 0.001$, one-way ANOVA with Tukey post-hoc comparison). The latency was increased in *unc13A* KD flies ($p < 0.001$, unpaired Student's t-test) and *unc13A* DN flies ($p < 0.01$, unpaired Student's t-test) as compared to controls. In **(a)**, **(c)**, and **(e)**, stimulus artifacts were minimized for clarity of presentation by linearly extrapolating between the pre- and post-stimulation artifact periods in Figure 5. Bar charts represent mean values.

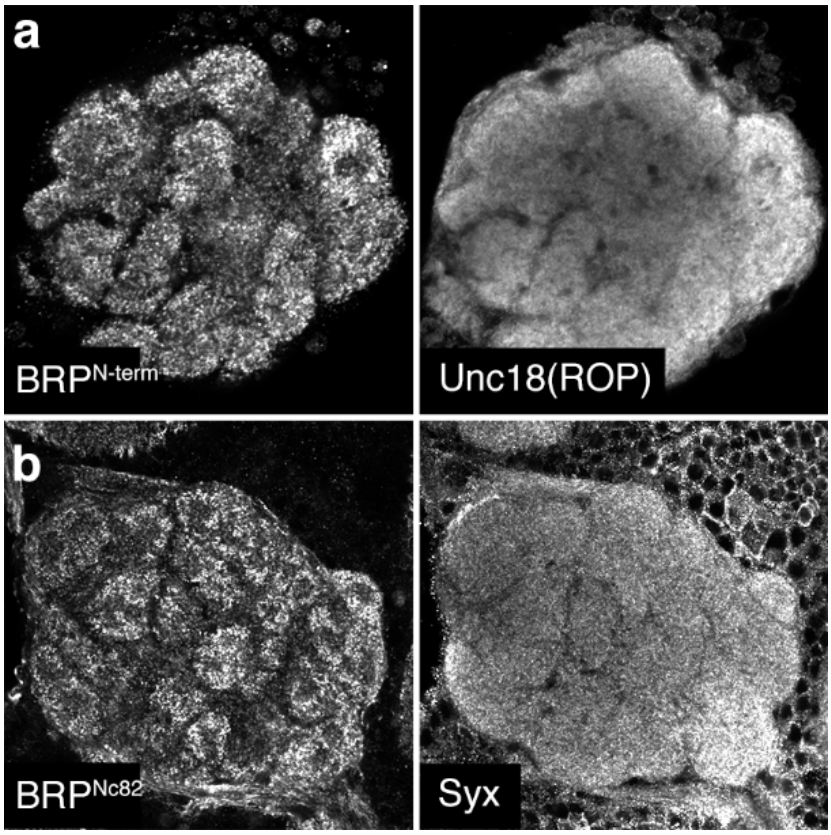

Figure S6: Distribution of the release factors Syntaxin (Syx) and Unc18 (ROP) in the AL, related to Figure 1
(a, b) Confocal sections of adult w^{1118} ALs.
(a) BRP N-term (left) and Unc18 (ROP) (right).
(b) BRP C-term (Nc82) (left) and Syntaxin (Syx) (right).

Supplemental Experimental Procedures

Resource Table

REAGENT or RESOURCE	SOURCE	IDENTIFIER
Antibodies		
Mouse monoclonal BRP^{Nc82}	DSHB; Wagh et al., 2006	Cat# nc82, RRID: AB_2314865
Guinea Pig Unc13A$^{N\text{-}term}$	Böhme et al., 2016	N/A
Rabbit Unc13B$^{N\text{-}term}$	Böhme et al., 2016	N/A
Guinea Pig Unc13B$^{N\text{-}term}$	This paper, self-raised	N/A
Rabbit Syd-1	Owald et al., 2010	N/A
Mouse ROP (Unc18)	DSHB	Cat# DSHB 4F8
Mouse Syntaxin	DSHB	Cat# DSHB 8C3
Chicken GFP	Abcam	Cat# ab13970
Rabbit BRP$^{N\text{-}term}$	Fouquet et al., 2009	N/A
Goat anti Mouse IgGs Alexa Fluor 488	Invitrogen	Cat# A21467
Goat anti Mouse IgGs Cy3	Abcam	Cat# ab102370
Goat anti Mouse IgGs Star635P	Abberior	Cat# 2-0002-007-5
Goat anti Rabbit IgGs Cy5	Invitrogen	Cat# A10523
Goat anti Rabbit IgGs Alexa Fluor 594	Invitrogen	Cat# A11037
Goat anti Guinea Pig IgGs Alexa Fluor 594	Invitrogen	Cat# A11076
Goat anti Chicken IgGs Alexa Fluor 488	Invitrogen	Cat# A21467
FluoTag X4 anti GFP Star635P	NanoTag Biotechnologies	Cat# N0304-Ab635P-L
Experimental Models: Organisms/Strains		
Drosophila: w^{1118} (control)	Hazelrigg et al., 1984	N/A
Drosophila: elav-GAL4 (X chromosome)	Lin and Goodman, 1994	N/A
Drosophila: MB247-GAL4	Zars et al., 2000	N/A
Drosophila: OR83b-GAL4 (ORCO-GAL4)	Wang et al., 2003	
Drosophila: GH146-GAL4	Bloomington	Cat# stock 30026
Drosophila: GMR-GAL4	Yamada et al., 2003	N/A
Drosophila: LN1^{NP1227}-GAL4	Das et al., 2008	N/A
Drosophila: mz19-GAL4	Ito et al., 1998	N/A
Drosophila: 17D-GAL4	Melzig et al., 1998	N/A
Drosophila: Pebbled-GAL4 (Pb-GAL4)	Nagel lab, NYU Sweeney et al., 2007	N/A
Drosophila: NP3056-GAL4,mCD8-GFP	Nagel lab, NYU	N/A
Drosophila: UAS-10xmCD8-GFP	Janelia Farm	N/A
Drosophila: UAS-brp-RNAi-B3,C8	Wagh et al., 2006	N/A
Drosophila: UAS-unc13A-RNAi-A1	This paper	N/A
Drosophila: UAS-unc13B-RNAi-B3	This paper	N/A
Drosophila: UAS-Cac-GFP	Liu et al., 2011	N/A
Drosophila: UAS-Brp^{short}-GFP	Christiansen et al., 2011	N/A
Drosophila: UAS-Unc13A^{Nterm}-GFP	Reddy-Alla et al., 2017	N/A
Drosophila: Syd-1 $^{ex1.2}$/Syd-1 $^{ex3.4}$	Owald et al., 2010	N/A
Drosophila: EMS7.5/P84200	Böhme et al., 2016	N/A
Drosophila: Del100BPacman/Del100BPacman; P84200/P84200	Böhme et al., 2016	N/A

Drosophila: Unc13Pacman/Unc13Pacman; P84200/P84200	Böhme et al., 2016	N/A
Drosophila: UAS-ChR2	Nagel lab, NYU	N/A
Oligonucleotides		
Unc13_B3-R: AATTCGCGATCCAACAAACTATCTTGATTATGCTTGAATATAACTAATCAAGATAGTTTGTTGGATCACTG	This paper	N/A
Unc13_B3-F: CTAGCAGTGATCCAACAAACTATCTTGATTAGTTATATTCAAGCATAATCAAGATAGTTTGTTGGATCGCG	This paper	N/A
Unc13_A1-R:AATTCGCGGGTTAGGACATAATAATCTATATGCTTGAATATAACTATAGATTATTATGTCCTAACCCACTG	This paper	N/A
Unc13_A1-F: CTAGCAGTGGGTTAGGACATAATAATCTATAGTTATATTCAAGCATATAGATTATTATGTCCTAACCCGCG	This paper	N/A
Unc13-IsoA-Nterm-Rev 5'- ATTAAGCTGCATGATTATTTTATTG-3'	This paper	N/A
Unc13-IsoA-Nterm-FW 5'- CACCATGACGCACTACGTGAGGC -3'	This paper	N/A
Software and Algorithms		
Amira	FEI	6.0.0
AutoQuant	MediaCybernetics	X2.2.2
Leica LAS X Software	Leica Microsystems	http://www.leica-microsystems.com/home/
Huygens	SVI	https://svi.nl/HomePage
ImageJ	NIH	1.51j
MATLAB	MathWorks	R2011a
R	R Foundation	3.3.3
SPSS Statistics	IBM	v20
Custom ImageJ plugins and R scripts	This paper	http://ratios.andlauer.net
Other		
TCS SP8 confocal microscope	Leica Microsystems	http://www.leica-microsystems.com
TCS SP8 gSTED 3x microscope	Leica Microsystems	http://www.leica-microsystems.com

Contact for reagent and resource sharing

Further information and requests for resources and reagents should be directed to and will be fulfilled by the lead contact, Stephan J. Sigrist (stephan.sigrist@fu-berlin.de).

Animal rearing and fly strains
Fly strains were reared under standard laboratory conditions (Sigrist et al., 2003) at 25 °C, 65-70% humidity and constant 12/12 hours light/dark cycle in incubators. The food recipe is based on the current Bloomington recipe for *Drosophila* medium (BDSC, 2017). If not stated differently, 4-7d female flies were used for the experiments.

Overview of the fly stocks used in this paper: w^{1118} (Hazelrigg et al., 1984), *elav-GAL4 (Lin and Goodman, 1994)*, *OR83b-GAL4* (*ORCO-GAL4*) (Wang et al., 2003), LN1-GAL4 (NP1227-GAL4) (Das et al., 2008), Mz19-GAL4 (Ito et al., 1998), 17D-GAL4 (Melzig et al., 1998), Pebbled-GAL4 (Pb-GAL4) (Sweeney et al., 2007), UAS-brp-RNAi-B3, UAS-brp-RNAi-C8 (Wagh et al., 2006), UAS-Cac^{GFP} (Liu et al., 2011), UAS-Brp^{short}-GFP (Christiansen et al., 2011), UAS-$Unc13A^{Nterm}$-GFP (Reddy-Alla et al., 2017), Syd-$1^{1.2}$/Syd-$1^{3.4}$ (Owald et al., 2010), EMS7.5/P84200 (Böhme et al., 2016), *Del100BPacman/Del100BPacman*; $Unc13^{P84200}$/$Unc13^{P84200}$ (Böhme et al., 2016), *Unc13Pacman/Unc13Pacman*; $Unc13^{P84200}$/$Unc13^{P84200}$ (Böhme et al., 2016). The $Unc13^{P84200}$ stock was obtained from Kyoto DGGR #101911. UAS-unc13A-RNAi-A1 and UAS-unc13B-RNAi-B3 are first published in this paper.

Experiment specific genotypes: If not stated otherwise, the strain used for general observations was w^{1118}. Genotypes used for deletions: $Unc13A^{null}$: $Unc13A^{EMS7.5}$/$Unc13^{P84200}$; $Unc13B^{null}$: *Del100BPacman/+;* $Unc13^{P84200}$/$Unc13^{P84200}$. Syd^{null}: $Syd^{ex1.2}$/$Syd^{ex3.4}$. Controls for all mutants: w^{1118}. Genotypes for knockdowns: Brp^{RNAi}*: elav-GAL4/+; UAS-brp-RNAi-B3,UAS-brp-RNAi-C8/+*. Controls: elav-GAL4/+; w^{1118}. Genotypes used for ratio experiments: *ORCO-GAL4/+; UAS-*Brp^{short}*-GFP/+. LN1-GAL4/+; UAS-*Brp^{short}*-GFP/+. Mz19-GAL4/+; UAS-*Brp^{short}*-GFP/+. 17D-GAL4/+; UAS-*Brp^{short}*-GFP/+. ORN-driven UAS-Cac-GFP: pb-GAL4/+; UAS-Cac-GFP/+*. Genotypes used for electrophysiology: *pb-GAL4/+; UAS-unc13A-RNAi-A1/+. pb-GAL4/+; UAS-unc13B-RNAi-B3/+. pb-GAL4/+; UAS-Unc13-Nterm-GFP. UAS-Unc13-Nterm-GFP, UAS-ChR2/+;NP3056-GAL4,UAS-mCD8-GFP/ UAS-unc13B-RNAi-B3. UAS-ChR2/+;NP3056-GAL4,UAS-mCD8-GFP/ UAS-unc13A-RNAi-A1. UAS-ChR2/+;NP3056-GAL4,UAS-mCD8-GFP/ +* (Control).

RNA interference
unc13 RNAi constructs were designed and cloned into *pWalium20* vectors, following the TRIP protocol from Harvard Medical School (Harvard medical school, 2017). Constructs were injected into *VK27 TM3(sb)* flies (Bloomington *Drosophila* stock center stock 9744) by BestGene (BestGene, Inc, Chino Hills, USA). The following primers were used:
Unc13-B3-Reverse:
AATTCGCGATCCAACAAACTATCTTGATTATGCTTGAATATAACTAATCAAGATAGTTTGTTGGATCACTG.
Unc13-B3-Forward:
CTAGCAGTGATCCAACAAACTATCTTGATTAGTTATATTCAAGCATAATCAAGATAGTTTGTTGGATCGCG.
Unc13-A1-Reverse:
AATTCGCGGGTTAGGACATAATAATCTATATGCTTGAATATAACTATAGATTATTATGTCCTAACCCACTG.
Unc13-A1-Forward:
CTAGCAGTGGGTTAGGACATAATAATCTATAGTTATATTCAAGCATATAGATTATTATGTCCTAACCCGCG.

Immunohistochemistry
Unless stated differently, 4-7d female fruit flies were used for the experiments. For *brp* knockdown experiments, 4-7d males raised on 29°C were utilized to boost RNAi efficacy.
The standard immunohistochemistry protocol illustrated below was slightly adjusted within the different experimental settings. Adult brains were dissected in ice-cold (HL3) solution, fixed for 40 min in 4% paraformaldehyde (PFA) in 1x phosphate-buffered saline (PBS), pH 7.2, at room temperature (RT), washed with 0.6 % Triton X-100 in 1x PBS (PBT) and blocked in 10% normal goat serum (NGS) in 0.6% PBT for 2 hrs at RT. The brains were incubated with primary antibodies together with 5% NGS in 0.6%

PBT for 48 hours at 4°C and then washed in 0.6% PBT for 3 hrs. (6x 30min after rinsing), followed by overnight incubation with secondary antibodies at 4°C. The brains were then washed for 3 hrs with 0.6% PBT and mounted in VectaShield (Vector Laboratories, Burlingame, USA) on glass slides. STED samples were mounted in ProLong® Gold Antifade Mountant (Invitrogen, Carlsbad, USA) with high precision cover slips No. 1.5H (Carl Roth GmbH & Co. KG, Karlsruhe, Germany).

Image acquisition

Conventional confocal images were acquired at constant 21°C with TCS SP8 confocal microscopes (Leica Microsystems, Wetzlar, Germany) using either a 63×, 1.4 NA oil or a 63×, 1.3 NA glycerin objective for detailed scans. For whole brain scans, either a 20×, 0.7 NA or a 40x, 1.3NA oil objective were used. The lateral pixel size was set to values around 100 nm for detailed scans. Typically, 1024 × 1024 pixel resolution images were scanned at 400 Hz using 3× line averaging for stacks, with lower scan speed and higher average for detailed single images. All images were acquired using the Leica LAS-X software. Deconvolution of images was conducted using AutoQuant X2.2.2 (MediaCybernetics, Rockville, USA). Confocal stacks were processed using ImageJ 1.51j (Schindelin et al., 2012a; Schneider et al., 2012). Contrast was adapted for visualization only, where necessary, using either the levels tool in Adobe Photoshop CC 2017.0.1 (Adobe, San José, USA) or ImageJ. Images shown in a comparative figure were processed with exactly the same parameters. Images were not post-processed before quantification, but exclusively afterwards and only for visualization.

STED microscopy was performed using a Leica Microsystems TCS SP8 gSTED 3x setup equipped with a pulsed white light laser (WLL; ~80-ps pulse width, 80-MHz repetition rate; NKT Photonics) and two STED lasers for depletion (continuous wave at 592 nm, pulsed at 775 nm). The pulsed 775 nm STED laser was triggered by the WLL. Images were acquired with a 100×, 1.4 NA oil immersion objective. 1024 × 1024 pixel resolution 2D STED images were scanned at 600 Hz using 8× line averaging. The lateral pixel size was set to values of ~20 nm, stacks of three images each were acquired, with a step size of 130 nm for a better estimation of the point spread function (PSF). To minimize thermal drift, the microscope was housed in a heatable incubation chamber. STED images were processed using the Huygens deconvolution software (SVI, Hilversum, The Netherlands) using a theoretical PSF automatically computed, based on a pulsed STED-optimized function and the specific microscope parameters. Default deconvolution settings were applied.

Quantification of average label intensities

Images were acquired as described above. For each dataset, fruit flies of different genotypes were dissected, treated, and processed equally and images were acquired with the same microscope/laser setting within the same scan session, alternating between different genotype groups to keep the conditions comparable. If a genotype comparison consisted of more than one dataset, values were normalized to the respective control group. Raw images were not altered or further processed prior to analysis. Average fluorophore intensities were analyzed using Amira 6.0.0 (FEI, Hillsboro, USA). Regions of interest (ROIs) were selected within the three-dimensional image stack using the Amira tool *Segmentation Editor*. The labels were optimized for all three fluorophore channels, excluding artifacts and non-neuropil staining. Mean intensity values within the 3D mask were calculated using the *Material Statistics* tool for all three channels. For background correction, mean intensities in non-neuropil regions (3D labels selected in the Brp^{NC82} channel) were subtracted from each individual neuropil value.

Background-corrected knockdown and deletion data were analyzed in *R* 3.3.3 with linear mixed models using the function *lmer* in the *R* package *lme4* (Bates et al., 2015). Animals were typically stained and imaged in several batches and 1-2 hemispheres per animal were scanned. Association of genotype with antibody levels was therefore tested using imaging batch and animal as nested random effects. In cases were the residuals of the model were not normally distributed (assessed via Shapiro-Wilk tests), the association was confirmed using a non-parametric permutation test using 10,000 permutations. If the permutation tests confirmed the results, the permutation test was not further mentioned in the text or figure legends. In case of deviations potentially influencing the significance level, the permutation test result is indicated. For the scaffold protein reduction experiment (Fig. 3), association tests were conducted using

linear mixed models with imaging batch and animal as nested random effects. A Bonferroni-corrected significance threshold of $\alpha = 0.0167$ was used for the *brp* KD and the *syd-1* deletion, and $\alpha = 0.025$ for the *unc13A/B* deletions.

STED distance analysis

GFP-labeled calcium channels (UAS-Cac-GFP) (Liu et al., 2011) were expressed in olfactory receptor neurons (ORNs) using the pb-GAL4 line (Sweeney et al., 2007). GFP-signals were enhanced using FluoTag®-X4 anti-GFP (NanoTag Biotechnologies GmbH, Göttingen, Germany) tagged with STAR 635p (Abberior, Göttingen, Germany). This fluorescent nanobody labels epitopes with a distance below 4 nm and each GFP is labeled with up to four fluorophores. GFP labels were combined with antibody stainings against either Unc13A or -B. All images within one dataset were acquired with the same microscope settings and deconvolved with Huygens (SVI, Hilversum, The Netherlands) using the same deconvolution parameters. Distances between fluorophores were analyzed using ImageJ 1.51j. STED channels for Cac-GFP and the respective Unc13 isoform were merged for each image (total size 19,39 × 19,39 μm). Twenty straight lines with a defined length of 400 nm were manually drawn through the centers of the signal from both channels in close proximity. Criteria for the selection of punctae were: Proximity closer than 400 nm, comparable relative intensity between the two channels, indicating the same Z position, and definite fluorophore spots. Lines were saved as regions of interests (ROIs). For analysis of peak-to-peak distances between the two fluorophore channels, the image-specific ROI sets were applied onto the STED channels and the 8-bit intensity values along the lines were detected using the *Fiji Multi-Plot* tool in the ROI manager. The distance between the intensity maxima of both channels was saved for each ROI as the distance for the respective analyzed AZ. The distances were analyzed using linear mixed models, as described above. Because several measurements were taken per image (scan), several images were scanned per hemisphere, and 1-2 hemispheres were analyzed per animal, scan, hemisphere, and animal were used as nested random effects.

Cluster distance and k nearest-neighbor analysis

For the cluster distance analysis, planar AZs were visually identified on deconvolved STED images of immunostainings against BRP^{NC82}. Several subregions of the image containing individual AZs were selected within 1 × 1 μm ROIs (53 × 53 pixels) in ImageJ v1.48v. The subregions were copied to new 1 μm^2 subimages for each channel. To identify the exact position of the AZ center, even smaller AZ ROIs were placed on the 1 μm^2 BRP^{NC82} subimages. AZ ROIs were rectangular, of variable size and chosen to be as small as possible yet at the same time to contain the full AZ as visible in the BRP signal. The starting positions $x_{AZ\text{-}ROI}$ and $y_{AZ\text{-}ROI}$ of each AZ ROI within the 1 μm^2 subimages was extracted using the *ImageJ* function *Roi.getBounds* and the AZ region within the AZ ROI was copied to a new image. The lowest intensity pixel was determined for each AZ region and its value subtracted from all pixel values in this image before the position of the AZ center was determined by calculating the coordinates ($x_{center\_of\_mass(AZ\text{-}image)}$ and $y_{center\_of\_mass(AZ\text{-}image)}$) of the center of mass, taking the pixel intensities into account and using output values XM and YM of the *ImageJ* function *Measure* (settings: mean min center redirect=None decimal=4). These coordinates identify the x and y position of the AZ center within the AZ ROI. To obtain the position of the AZ center in the context of the larger, 1 μm^2 subimages, the position of AZ ROIs within the 1 μm^2 ROI was taken into account ($x_{AZ\text{-}center(1\mu m^2\text{-}image)}=x_{center\_of\_mass(AZ\text{-}image)}+x_{AZ\text{-}ROI}$ and $y_{AZ\text{-}center(1\mu m^2\text{-}image)}=y_{center\_of\_mass(AZ\text{-}image)}+y_{AZ\text{-}ROI}$). To investigate the spatial relation of Unc13A or Unc13B to the AZ center, the same 1 μm^2 ROIs were used in the second channel as had been used for the first one. The position of protein spots was determined by first detecting local intensity maxima using the *ImageJ* function *Find maxima* (noise=5 output=[PointSelection]), followed by identifying their positions using the output values “X” and “Y” of the *ImageJ* function *Measure* (settings: “mean centroid center limit display redirect=None decimal=4”). Our procedure allowed reading out up to 50 such spots per AZ, but in reality, far fewer (roughly 20 in the case of Unc13A and of Unc13B) were detected.

Subsequently, the distance of protein spots to the AZ center was calculated using *Matlab* (v7.12.0.635 R2011a 64 bit, Mathworks, Natick, USA). The Euclidean distance of Unc13A and Unc13B spots to the center of mass of the BRP^{NC82} staining was determined. For each AZ, the observed distances were ranked and the minimum distance selected. Furthermore, the number of observed spots within distance bins from the BRP ring center (0-50 nm, 50-100 nm, 100-150 nm and 150-200 nm) was counted and

divided by the total number of either Unc13A or Unc13B spots found within a 200 nm radius. To obtain estimates for the entire brain, all values retrieved were averaged across all AZs per brain.
Statistical tests were conducted in SPSS (IBM, Armonk, USA). Normality of data was tested with the Shapiro-Wilk test and by inspection of histograms and QQ plots. The nonparametric Mann Whitney U test was used for analyses. Graphs show medians, interquartile ranges and min/max values and n indicates the number of animals tested.

Electrophysiology
Whole-cell patch-clamp recordings from PNs and LNs were made as described (Nagel et al., 2015; Nagel and Wilson, 2016). Female flies, 1-2 days post-eclosion, were positioned in a horizontal platform, with the dorsal part of the fly head above the platform and most of the fly below the platform. The dorsal part of the fly head was dissected to expose the brain and bathed in external saline containing 103 mM NaCl, 3 mM KCl, 5 mM TES, 8 mM trehalose, 10 mM glucose, 26 mM $NaHCO_3$, 1 mM NaH_2PO_4, 4 mM $MgCl_2$ and 1.5 mM $CaCl_2$. Cell bodies were visualized using infrared optics and a 40× water-immersion objective on an upright compound microscope (Olympus BX51). Patch pipettes (6-8 MΩ) were pulled the day of the recording and filled with internal solution containing 140 mM CsOH, 140 mM aspartic acid, 10 mM HEPES, 1 mM EGTA, 1 mM KCl, 4 mM MgATP, 0.5 mM Na_3GTP, 5 mM QX-314•Cl^- and 13 mM biocytin hydrazide. For current clamp recordings from presynaptic LNs KOH was used instead of CsPH. The pH of the internal solution was adjusted to 7.2 ± 0.1 and osmolarity to 265 ± 3 mOsm. PNs were identified by characteristic location and size within the antennal lobe. PNs with input resistance less than 500 MΩ or greater than 1200 MΩ were excluded from analysis, as were PNs in which an EPSC could not be elicited by 100 μA of current injection into the antennal nerve. To electrically stimulate presynaptic ORN axons, the antennae were removed and the ipsilateral antennal nerve was drawn into a large diameter pipette filled with saline. The nerve bundle was stimulated using a WPI stimulus isolator in constant current mode, with intensities ranging from 10 – 100 μA. The stimulus intensity was adjusted to the minimum amplitude that reliably elicited an EPSC on the first pulse. For LN recordings, channel rhodopsin was stimulated with 470 nm light through the microscope objective. We first made current clamp recordings from GFP+ LNs and adjusted light intensity so that robust spiking was obtained. The same intensity settings were used for GFP-LN recordings in voltage clamp. LNs were identified based on morphology and electrophysiological properties. After voltage clamp experiments, the identity of LNs was confirmed by switching briefly to current clamp mode and observing the waveforms of spontaneous spikes. Comparisons between groups were performed with a Kruskal-Wallis or one-way ANOVA test as indicated in the text. In the quantification of paired-pulse ratios (Figure 5), one *unc13B* KD recording was excluded from this analysis because no EPSC was produced in response to the first stimulation pulse.

Ratiometric analysis of presynaptic proteins
Ratios between two presynaptic antibody signal intensities were calculated for each pixel of three-channel, 8-bit, three-dimensional image stacks using custom *ImageJ* plugins (http://ratios.andlauer.net). First, the respective neuropil of interest (AL or calyx) was segmented from the rest of the brain using the *Fiji ImageJ* plugin *Segmentation Editor* (Christiansen et al., 2011; Schindelin et al., 2012b). A second mask was generated for GFP-positive voxels within the neuropil of interest. Second, we applied a percentile threshold to each image to remove unspecific background staining (non-AZ signal) from the masked regions. Voxels below the threshold were set to an intensity value of zero. For analysis of whole neuropils, the percentile threshold was 0.8, for the analysis of GFP-positive voxels 0.95. Because intensities vary within image stacks, each stack was divided into substacks for the determination of optimal absolute intensity value thresholds. Third, voxelwise ratio values were calculated. All oversaturated voxels (absolute intensity 255) were omitted from the calculation of ratio-based statistics. For visualization, ratios were ranked and mapped to a false-color gradient. This allowed for highlighting of synapse populations with especially strong differences in AZ protein intensity. Fourth, weighted median ratios were calculated on real (non-ranked) ratio values in *R* v3.3.3, once for the whole neuropil and once for the GFP-positive areas. For normalization, median ratios of GFP-positive voxels were divided by median ratios of the whole neuropil. Normalized median ratios were compared using Mann-Whitney U tests. The source code of all *ImageJ* plugins and the *R* scripts are available for download at http://ratios.andlauer.net.

Colocalization analysis
Colocalization analyses were conducted using the *Fiji Coloc 2* plugin (https://imagej.net/Coloc_2). The colocalizations between pairs of two antibodies in single image planes of triple stainings were analyzed using Spearman correlation. Spearman rank correlation coefficients were compared using the paired Wilcoxon signed-rank test.

Supplemental References

Bates, D., Mächler, M., Bolker, B., and Walker, S. (2015). Fitting Linear Mixed-Effects Models Using lme4. 2015 *67*, 48.

BDSC (2017). Bloom Food - Bloomington.

Böhme, M.A., Beis, C., Reddy-Alla, S., Reynolds, E., Mampell, M.M., Grasskamp, A.T., Lutzkendorf, J., Bergeron, D.D., Driller, J.H., Babikir, H.*, et al.* (2016). Active zone scaffolds differentially accumulate Unc13 isoforms to tune Ca(2+) channel-vesicle coupling. Nature neuroscience *19*, 1311-1320.

Christiansen, F., Zube, C., Andlauer, T.F., Wichmann, C., Fouquet, W., Owald, D., Mertel, S., Leiss, F., Tavosanis, G., Luna, A.J.*, et al.* (2011). Presynapses in Kenyon cell dendrites in the mushroom body calyx of Drosophila. J Neurosci *31*, 9696-9707.

Das, A., Sen, S., Lichtneckert, R., Okada, R., Ito, K., Rodrigues, V., and Reichert, H. (2008). Drosophila olfactory local interneurons and projection neurons derive from a common neuroblast lineage specified by the empty spiracles gene. Neural Dev *3*, 33.

Harvard medical school (2017). Cloning and sequencing.

Hazelrigg, T., Levis, R., and Rubin, G.M. (1984). Transformation of white locus DNA in Drosophila: Dosage compensation, zeste interaction, and position effects. Cell *36*, 469-481.

Ito, K., Suzuki, K., Estes, P., Ramaswami, M., Yamamoto, D., and Strausfeld, N.J. (1998). The organization of extrinsic neurons and their implications in the functional roles of the mushroom bodies in Drosophila melanogaster Meigen. Learn Mem *5*, 52-77.

Lin, D.M., and Goodman, C.S. (1994). Ectopic and increased expression of Fasciclin II alters motoneuron growth cone guidance. Neuron *13*, 507-523.

Liu, K.S., Siebert, M., Mertel, S., Knoche, E., Wegener, S., Wichmann, C., Matkovic, T., Muhammad, K., Depner, H., Mettke, C.*, et al.* (2011). RIM-binding protein, a central part of the active zone, is essential for neurotransmitter release. Science (New York, NY) *334*, 1565-1569.

Melzig, J., Rein, K.H., Schafer, U., Pfister, H., Jackle, H., Heisenberg, M., and Raabe, T. (1998). A protein related to p21-activated kinase (PAK) that is involved in neurogenesis in the Drosophila adult central nervous system. Curr Biol *8*, 1223-1226.

Nagel, K.I., Hong, E.J., and Wilson, R.I. (2015). Synaptic and circuit mechanisms promoting broadband transmission of olfactory stimulus dynamics. Nat Neurosci *18*, 56-65.

Nagel, K.I., and Wilson, R.I. (2016). Mechanisms Underlying Population Response Dynamics in Inhibitory Interneurons of the Drosophila Antennal Lobe. J Neurosci *36*, 4325-4338.

Owald, D., Fouquet, W., Schmidt, M., Wichmann, C., Mertel, S., Depner, H., Christiansen, F., Zube, C., Quentin, C., Korner, J.*, et al.* (2010). A Syd-1 homologue regulates pre- and postsynaptic maturation in Drosophila. J Cell Biol *188*, 565-579.

Reddy-Alla, S., Böhme, M.A., Reynolds, E., Beis, C., Grasskamp, A.T., Mampell, M.M., Maglione, M., Jusyte, M., Rey, U., Babikir, H.*, et al.* (2017). Stable Positioning of Unc13 Restricts Synaptic Vesicle Fusion to Defined Release Sites to Promote Synchronous Neurotransmission. Neuron *95*, 1350-1364.e1312.

Schindelin, J., Arganda-Carreras, I., Frise, E., Kaynig, V., Longair, M., Pietzsch, T., Preibisch, S., Rueden, C., Saalfeld, S., Schmid, B.*, et al.* (2012a). Fiji: an open-source platform for biological-image analysis. Nature Methods *9*, 676-682.

Schindelin, J., Arganda-Carreras, I., Frise, E., Kaynig, V., Longair, M., Pietzsch, T., Preibisch, S., Rueden, C., Saalfeld, S., Schmid, B.*, et al.* (2012b). Fiji: an open-source platform for biological-image analysis. Nat Methods *9*, 676-682.

Schneider, C.A., Rasband, W.S., and Eliceiri, K.W. (2012). NIH Image to ImageJ: 25 years of image analysis. Nature Methods *9*, 671-675.

Sigrist, S.J., Reiff, D.F., Thiel, P.R., Steinert, J.R., and Schuster, C.M. (2003). Experience-dependent strengthening of Drosophila neuromuscular junctions. J Neurosci *23*, 6546-6556.

Sweeney, L.B., Couto, A., Chou, Y.-H., Berdnik, D., Dickson, B.J., Luo, L., and Komiyama, T. (2007). Temporal Target Restriction of Olfactory Receptor Neurons by Semaphorin-1a/PlexinA-Mediated Axon-Axon Interactions. Neuron *53*, 185-200.

Wagh, D.A., Rasse, T.M., Asan, E., Hofbauer, A., Schwenkert, I., Durrbeck, H., Buchner, S., Dabauvalle, M.C., Schmidt, M., Qin, G.*, et al.* (2006). Bruchpilot, a protein with homology to ELKS/CAST, is required for structural integrity and function of synaptic active zones in Drosophila. Neuron *49*, 833-844.

Wang, J.W., Wong, A.M., Flores, J., Vosshall, L.B., and Axel, R. (2003). Two-photon calcium imaging reveals an odor-evoked map of activity in the fly brain. Cell *112*, 271-282.

Yamada, T., Okabe, M., and Hiromi, Y. (2003). EDL/MAE regulates EGF-mediated induction by antagonizing Ets transcription factor Pointed. Development *130*, 4085-4096.

Zars, T., Fischer, M., Schulz, R., and Heisenberg, M. (2000). Localization of a short-term memory in Drosophila. Science *288*, 672-675.